# Electrical-to-Mechanical Coupling in Purple Membranes: Membrane as Electrostrictive Medium

Povilas Kietis,*† Mikas Vengris,† and Leonas Valkunas†
*Physics Faculty, Vilnius University, 2054 Vilnius and †Institute of Physics, 2600 Vilnius, Lithuania

ABSTRACT In this paper, we present acousto-electrical measurements performed on dry films of purple membranes (PM) of *Halobacterium salinarium*. The purpose of these measurements is to determine the relation between mechanical and electrical phenomena in bacteriorhodopsin and to define the role of the protein in the proton transfer process. Electrical-to-mechanical coupling in PMs manifests itself as direct and inverse piezoelectric effects. Measurements performed on the samples with different degrees of PM orientation and at various values of the externally applied cross-membrane electric field indicate that piezoelectric phenomena in PMs arise from the electric asymmetry of the membranes, i.e., they originate from electrostriction. Experiments with samples made of oriented PMs allow estimation of the value of the intrinsic cross-membrane electric field, which is $\approx 10^8$ V/m. A hypothetical model of PM is presented where the electrical-to-mechanical coupling is suggested to be the main driving force for the proton translocation against the Coulomb forces acting in the membrane.

## INTRODUCTION

Bacteriorhodopsin (BR) from the purple membrane of *Halobacterium salinarium* is the simplest membrane protein performing the active transmembrane proton pumping. Knowledge of the structural organization of the BR with less than 3-Å resolution (see recent data: Kimura et al., 1997; Essen et al., 1998; Luecke et al., 1999; Belrhali et al., 1999) enables relation of the details in structural changes to the intermediate states in proton transportation from the intracellular to extracellular sides of the membrane. These intermediates of the photocycle, denoted as J, K, L, M, N, and O are well spectroscopically detectable according to their absorption maxima in various spectral regions (see Mathies et al., 1991; Rothschild, 1992; Oesterhelt et al., 1992; for review). These intermediates arise and decay sequentially after the photon absorption by retinal—the chromophore of BR, which is covalently bound to the protein via a protonated Schiff base linkage. Thus, the process of the proton pumping initiated by *trans*-to-*cis* isomerization of the retinal immediately after absorption of the photon is driven by deprotonation of the Schiff base in the M intermediate (Varo and Lanyi, 1991). This conclusion is based on spectroscopic results obtained by various experimental techniques, such as visible, ultraviolet, resonance Raman, and Fourier-transformed infrared spectroscopy (see Lanyi, 1993; for the review), and nuclear magnetic resonance (de Groot et al., 1989, 1990) and by using mutants of BR (Brown et al., 1995; Balashov et al., 1997; Lu et al., 2000). BR has been studied by changing the external conditions, such as pH (Zimanyi et al., 1992; Heberle and Dencher, 1992; Cao et al., 1995; Ludmann et al., 1998b), and the amount of water (Popp et al., 1993; Ganea et al., 1997). These studies allowed monitoring of the retinal chromophore by using its sensitivity to the (protonated/deprotonated) state of the Schiff base and to follow details of the time-course of the proton exchange between particular groups of the protein and between the protein and its surrounding.

Together with spectroscopic measurements, which allow determination of the transition rates between different intermediates, electric measurements reveal the electrogenicity of the intermediates in the course of the proton transport, which is directly related to the functional aspect of BR (Trissl, 1990; Wang et al., 1997; Ludmann et al., 1998a). Despite of the details in the sequence of proton transfer through the protein in the course of photocycle of BR, the mechanism resulting in the driving force of this process still remains obscure.

The active transport of protons in BR and the increase in the electric conductivity of the purple membranes stimulated by light are usually considered as separate phenomena, not related to each other on the common physical ground. The conductivity problem is, in general, more complex, because, in addition to the proton transfer via the intermediate states, it can also be sensitive to reorganization of internal charged groups and dipoles present in the protein. BR rapidly reacts to the externally imposed electric field: the field causes a protein deformation, as recently demonstrated by atomic force microscopy (Rousso et al., 1997a,b). These studies have shown that the protein dynamics initiated by the absorption of light causes the initial increase in the volume of the protein with a subsequent decrease in it on the microsecond/millisecond time scale. According to our recent suggestions (Kietis et al., 1998a), such protein dynamics can also be related to the driving force for the proton pumping performed by the protein. This suggestion was based on linear (Kietis, 1984; Kietis and Rozga, 1987) and

*Received for publication 9 August 2000 and in final form 19 December 2000.*

Address reprint requests to Leonas Valkunas, Institute of Physics, A. Gostauto 12, Vilnius 2600, Lithuania. Tel.: 3702-612610; Fax: 3702-617070; E-mail: valkunas@ktl.mii.lt.



0006-3495/01/04/1631/10 $2.00

nonlinear (Kietis et al., 1998b) piezoelectric properties of BR. However, the origin of piezoelectricity of BR still remains unclear.

In this paper, we present the studies of mechanical-to-electrical coupling phenomena in purple membranes. The main purpose of these studies is to determine the origin of protein dynamics initiated by the externally applied electric field and, especially, to establish the possible role of the protein in the proton pumping. We discuss how the feedback of the protein to the electronic excitation of retinal can result in the driving force for the proton transfer against the Coulomb forces acting in the membrane.

It is shown that electrostriction is inherent in BR and, moreover, the presence of the transmembrane electric field allows understanding of the origin of the piezoelectricity discovered in these systems. It is noteworthy that electrostriction was observed in other ion channels as well (Pasechnik, 1982). Therefore, together with the experimental analysis of the results obtained for the BR films, a more general discussion relating the mechanism of the proton pumping is also presented.

## MATERIALS AND METHODS

### Sample preparation

Non-oriented films of purple membranes (PM) were produced by dropping the PM suspension on the rotating glass tray covered with the same layer of $SnO_2$. The thickness of the film was estimated from the optical density ($D$) using the relation $D = n\kappa d$, where $n$ is the molar concentration of chromophores, $\kappa$ is the extinction coefficient ($\kappa = 6.3 \times 10^3$ m$^2$/M for BR at 570 nm), and $d$ is the thickness of the film. By substituting the concentration $n$ (calculated as the inverse of the BR molecule volume divided by the Avogadro number) it can easily be shown that the thickness of the film with the optical density of 2 optical units is $\approx$14 $\mu$m. The optical density of the film was adjusted to $D \approx 2$ optical units by repeatedly dropping the suspension and drying it layer by layer.

Oriented films of PM containing BR were electrophoretically precipitated on a glass plate coated with a $SnO_2$ layer according to the standard procedure (Varo, 1981). The area of the film surface was 0.5 cm$^2$ in size. The $SnO_2$ layer served as a light-transparent electrode for measuring the optical density and the photoelectric potential of the film. The load resistance of the potential measuring equipment was chosen to be $10^{12}$ $\Omega$.

The voltage generated by the actinic light ($\lambda$ = 570 nm, illumination intensity around 400 W/m$^2$), is in the range from 5 to 15 V depending on a particular PM film. This variation is attributed to the differences in the degree of orientation of PMs in various films and thus can be used for the estimation of the latter value. The films with resulting voltage close to zero were classified as "non-oriented," those providing voltages around 5 V were identified as "weakly oriented" or "partly oriented" and the films whose voltages were close to 15 V, were treated as "highly" or "totally" oriented. It is worthwhile to mention that the orientation degree of the films is even visually distinguishable because the oriented films turned to have a bluish color. This is caused by the increased acidity (Oesterhelt and Stoeckenius, 1971), which results from the dissociation of water molecules in the vicinity of the electrode used for electrophoresis. Thus, in our preparation procedure, the pH of the samples is related to their degree of orientation (oriented films were prepared under the conditions with lower pH than non-oriented ones).

### Experimental

For direct and indirect electromechanical response of PM films, a home-built setup, schematically shown in Fig. 1, was used. The AC voltage from the oscillator producing the 1.2-MHz harmonic signal $U_{1\sim}$ with the amplitude $U_{10} < 2$V was applied on the film. The DC voltage source was also applied for the generation of the bias signal $U_0$ in the interval from $-80$ to 80 V. Here, the sign of the voltage has a meaning in the case of oriented (asymmetric) PM films only. It corresponds to the positive voltage connected to the external side of the membrane (see Fig. 1). The harmonic deformation $S_\sim$ of the film resulted from electrostriction or piezoelectricity (Kietis et al., 1999) was directed by the glass waveguide to the $BaTiO_3$ piezoelectric transducer (PET) with the resonance frequency equal to that of the external harmonic signal, i.e., 1.2 MHz. Static (time-independent) deformations of the PM film have no influence on the PET.

To improve the acoustic contact between the film and the waveguide, the latter was moistened with the transformer oil. The $BaTiO_3$ converter is sensitive to the longitudinal acoustic modes and generates the electric signal $U_{2\sim}$. The DC voltage $U_0$ generates static deformation, which has no influence on the PET. However, by changing $U_0$, it is possible to scan the volt-deformational characteristic of the film. If this characteristic is nonlinear, the transformation function of the AC signal,

$$k_{1\to2}(U_0) = U_{20}/U_{10}, \tag{1}$$

is dependent on the DC voltage $U_0$. Here $U_{20}$ denotes the amplitude of the $U_{2\sim}$ signal and $U_{10}$ is the amplitude of $U_{1\sim}$. From this dependence, volt-deformation characteristics of the film can be obtained using the following arguments.

By imposing both the DC ($U_0$) and AC ($U_{1\sim} = U_{10}\cos\omega t$) voltages, the resulting voltage creating the deformation $S = S(U)$ then is a sum of both values, i.e., $U = U_0 + U_{1\sim}$. In the case of a weak AC field ($U_{10} \ll U_0$), the amplitude of the deformation $S_0$ can be estimated as

$$S_0 = \left.\frac{dS}{dU}\right|_{U=U_0} U_{10}. \tag{2}$$

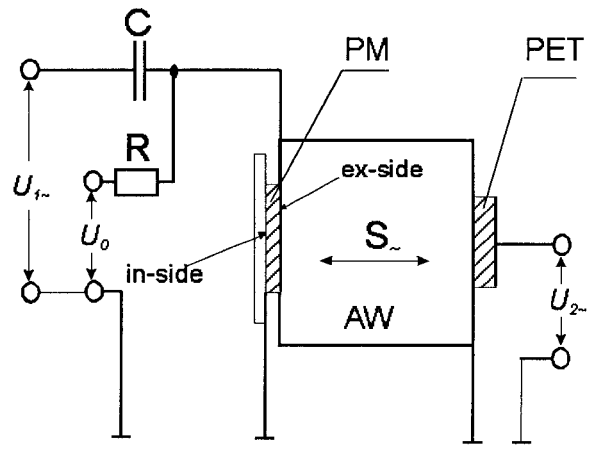


FIGURE 1 Experimental setup. *PM*, the film of dry purple membranes with electrodes connected to the surfaces; *AW*, the acoustic waveguide; *PET*, $BaTiO_3$ piezoelectric transducer. AC voltage $U_{1\sim}$ is imposed on the sample via the capacitor $C$ (100 pF). Bias voltage $U_0$ is connected to the resistor $R$ (100 k$\Omega$). The response to the external electric field is obtained as $U_{2\sim}$. The response to the external deformation is measured with the AC voltage supplied as $U_{2\sim}$. Then the resulting DC and AC components of the sample response are measured as $U_0$ and $U_{1\sim}$ (for details see text).

The latter relationship enables us to determine experimentally the derivative of the unknown deformation function at a fixed value of the applied voltage $U_0$ as a ratio $S_0/U_{10}$. Because the PET signal $U_{20}$ is proportional to the deformation, i.e., $U_{20} \sim S_0$, by considering also Eqs. 1 and 2, we can derive the deformation function $S$ from the dependence of the transformation coefficient $k_{1\to2}(U_0)$ on the bias voltage,

$$S(U_0) \sim \int k_{1\to2}(U_0)\, dU_0 + \text{const}, \qquad (3)$$

where the integration constant can be determined from the chosen boundary condition. The natural boundary condition in our case is to set the deformation equal to zero at the bias value where the transformation function is zero. Eq. 3 describes the general dependence of the deformation on the applied voltage, i.e., it defines the volt-deformation characteristic of the PM film.

When the external AC signal with the frequency of 1.2 MHz is imposed on PET, the latter becomes a source of the acoustic waves, which stimulate the deformation of the film. If the film has inherent piezoelectric properties, the electric signal appears between the electrodes connected to the surfaces of the film. This scheme of the measurement corresponds to studies of the direct piezoelectric effect, whereas the previous description of the scheme allows detection of the so-called inverse piezoelectric effect.

## RESULTS

### Inverse piezoelectric effect in PM films

The dependence of the transformation function defined by Eq. 1 on the DC voltage $U_0$ is shown in Fig. 2 for the films with the different degrees of the PM orientation. The phase difference of 180° between the input signal $U_{1\sim}$ and the detected signal $U_{2\sim}$ is reflected in the data by the minus sign of the transformation function. Evidently, at the values of the bias voltage, where the flip of this phase difference occurs, the transformation function is zero. The position of this zero-crossing point on the $U_0$ axis depends on the degree of orientation of PMs and is well distinguished for non-oriented and weakly oriented films. In the case of highly oriented films, this point could not be reached because it is at $U_0 > 100$ $V$, i.e., at values of the electric field higher than those where the electrical damage of the sample occurs. By integrating the experimentally obtained transformation function according to Eq. 3 and considering phase changes of the signal, the volt-deformation characteristics of the films with different degrees of PM orientation are obtained (see Fig. 3). Because the measured signal $U_{2\sim}$ is proportional to the deformation of the film $S_\sim$, the results are presented in arbitrary units. It is noteworthy that the volt-deformation characteristic of non-oriented films is a parabolic function, symmetric with respect to the point $U_0 = 0$. From the comparison of the response of PM films with the known piezoelectric material (e.g., quartz crystal), we determine the sign of the deformation. It appears that both positive and negative external fields create positive deformation (the thickness of the film decreases). The increase in the degree of the PM orientation in the film shifts the minimum of the parabolic characteristic toward the positive values of $U_0$. As already mentioned, this minimum is not reachable in the case of highly oriented films because of the electric damage to the sample.

For comparison, the same kind of measurements were also carried out with some other films or plates of the same thickness. For instance, the transformation coefficient $k_{1\to2}$ for mica plate is obtained to be zero within the sensitivity of our experimental equipment, whereas the polyethylene film generates the signal $U_{2\sim}$, which has a similar dependence on the bias voltage $U_0$ as is obtained for non-oriented films of PMs. Thus, it is noteworthy that the shift of the minimum of the parabolic characteristics of the deformation along the $U_0$ axis (see Fig. 3) is obtained for the oriented PMs only.

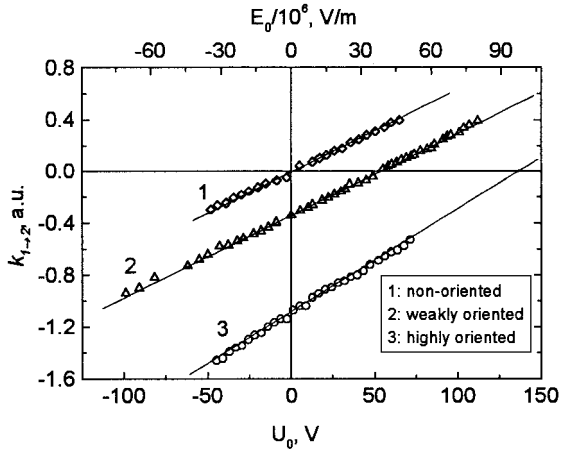


FIGURE 2 The dependence of the electrical-to-acoustical transformation function in non-oriented (*1*, *diamonds*), partly (*2*, *triangles*), and highly (*3*, *circles*) oriented PM films on the applied bias voltage $U_0$. On the top axis, the values of the bias voltage are given recalculated into the cross-membrane electric field ($E_0 = U_0/d$). Positive values of the electric field $E_0$ mean that the electric field is directed from the external to the internal side of the membrane. Negative values of the transformation function indicate that the phase difference between excitation and detection signals is 180°. Solid lines depict linear approximations of the measured datasets.

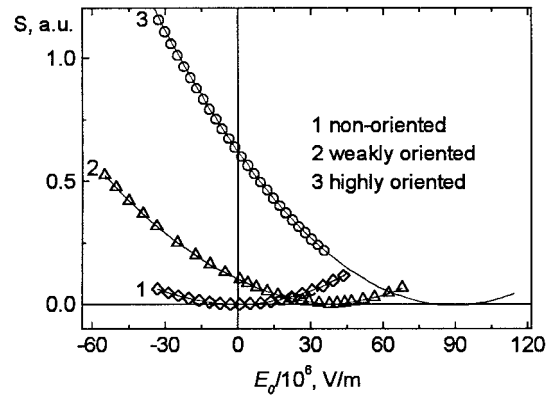


FIGURE 3 Deformation of PM films with various degrees of orientation plotted as a function of the cross-membrane electric field. Notations as in Fig. 2.

Volt-deformation characteristics shown in Fig. 3 are evidently nonlinear. This means that the sample can generate higher harmonics of the excitation signal. Therefore, measurements directed to detect the second harmonics have been carried out. When the PM film is excited by the AC voltage $U_{1\sim}$ at 600 kHz, and PET is tuned to 1.2 MHz, the second harmonic signal is obtained as $U_{2\sim}$. For all types of the films, the ratio between amplitudes of the second harmonic ($U_{20}$) and the excitation signal ($U_{10}$) does not depend on $U_0$ (see Fig. 4), whereas the value $U_{20}$ itself shows a quadratic dependence on the amplitude of the excitation signal $U_{10}$ (see Fig. 5). The latter allows us to conclude that the volt-deformation characteristics are completely defined by the quadratic dependence on the external DC field. The difference between the oriented and non-oriented films can be attributed to the differences in electromechanical properties of these films.

### Direct piezoelectric effect in PM films

The direct piezoelectric effect is also inherent in the PM films. This can be observed by using the same equipment shown in Fig. 1 by connecting the excitation voltage $U_{2\sim}$ to the PET at 1.2 MHz frequency. The acoustic wave is then generated that propagates through the waveguide (*AW* in Fig. 1) and deforms the PM film. If the film has inherent piezoelectric properties, the electric signal $U_{1\sim}$ appears on the electrodes connected to the surfaces of the film. The dependence of such electric response (with the corresponding transformation function $k_{2\to1} = U_{10}/U_{20}$, which is similarly defined as in Eq. 1) on the applied DC external voltage is shown in Fig. 6. From comparison of the results with those presented in Fig. 2, it is evident that direct and inverse mechanical-to-electrical effects disappear at the same values of $U_0$ for the films with the same degree of orientation. This is a direct indication that both effects are of the same origin.

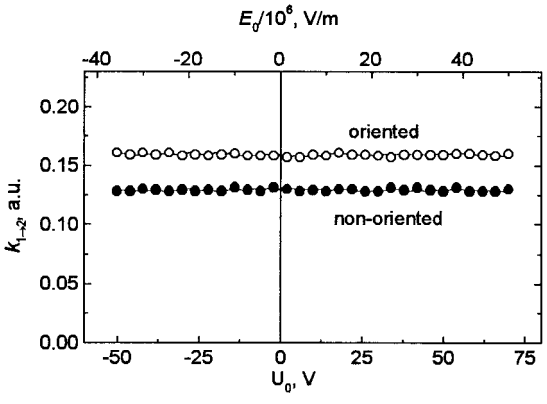


FIGURE 4 Frequency-doubling efficiency of PM films plotted as a function of the applied bias voltage. The top axis shows the bias values recalculated into the cross-membrane electric field.

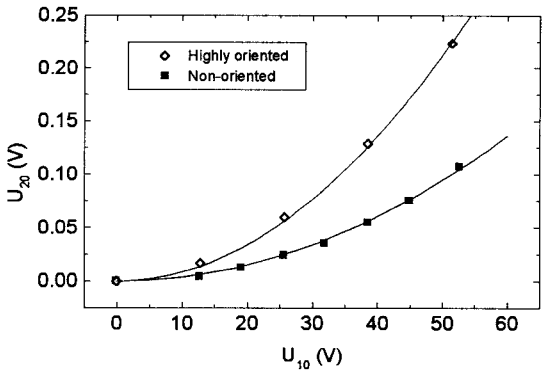


FIGURE 5 Dependence of the second harmonic amplitude $U_{20}$ on the amplitude of the input signal $U_{10}$. Solid lines show the fits of the measured datasets with parabolic functions.

## DISCUSSION

The quadratic dependence of the deformation on the external electric field (see Fig. 3) revealed by the measurements of the indirect piezoelectric effect can be explained in terms of the electrostriction effect, which determines the electromechanical properties of BR. Differences in the experimental results yielded by the films with different degrees of orientation are interpreted in terms of the presence of the internal cross-membrane electric field. This is the basic concept used for the interpretations of the experimental data.

### Inverse piezoelectric effect

The shift of the minimum of the transformation function along the $U_0$ (or $E_0$) axis depending on the degree of

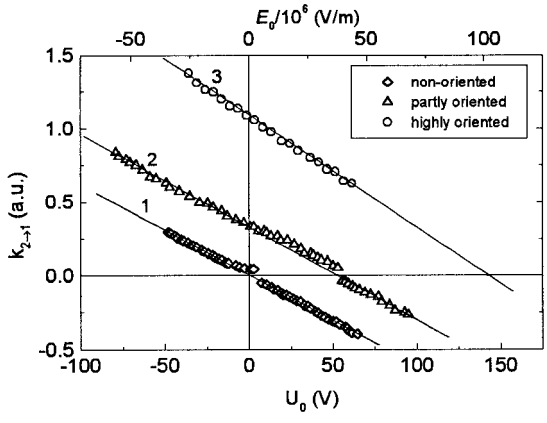


FIGURE 6 Electrical response of PM films with different degrees of orientation to the external deformation plotted as a function of the external bias voltage $U_0$. The response $k_{2\to1}$ is obtained as the ratio of amplitudes of the AC voltage $U_{2\sim}$ applied on the PET and $U_{1\sim}$ measured on the surfaces of the PM film. On the top axis, the values of the bias voltage are recalculated into the values of the cross-membrane electric field. Notations as in Fig. 2.

orientation (see Fig. 2) can be attributed to the internal electric field present in the PM. This field can result from the dipole moment of the BR molecule, or, macroscopically speaking, from the electric asymmetry of a separate PM. In non-oriented films, the internal electric fields compensate each other, resulting in the overall zero electric field, and, thus, the parabola shown in Fig. 3 is symmetric with respect to $E_0 = 0$. This compensation effect is evidently absent in partly or highly orientated films, and, consequently, the resultant electric field across the film is nonzero. The external DC voltage applied compensates this resultant electric field. In the experiment, this manifests itself as a shift of the corresponding parabola along the $E_0$ axis.

These observations can be understood in terms of electrostriction (see Appendix and Landau and Lifshitz, 1960, for details). On the basis of the above, let us assume now that PM films compose a mixture of two fractions characterized by different (opposite to each other) orientations of the resultant electric field with respect to the external field. Then the resulting electric field in the film can be determined as

$$E = E_0 + E_{1\sim} + \alpha E_m - (1 - \alpha)E_m, \tag{4}$$

where $E_m$ is the intrinsic electric field of a single membrane and $\alpha$ is the fraction of membranes in the film oriented so that their electric field is directed along $E_0$. For our experimental conditions, the electric field $E_{1\sim} = U_{1\sim}/d$ created by the AC external voltage $U_{1\sim}$ can be written as $E_{1\sim} = E_{10} \cos \omega t$. By substituting Eq. 4 into Eq. A.3 and neglecting time-independent terms that determine the static deformation (the latter is not registered by the PET), the variable deformation can be determined as

$$S_\sim = \frac{\xi}{c}\left\{[E_0 + (2\alpha - 1)E_m]E_{10}\cos \omega t + \frac{1}{2}E_{10}^2 \cos 2\omega t\right\}, \tag{5}$$

where $c$ is the elasticity of the PM and $\xi = \varepsilon_0\rho(d\varepsilon/d\rho)$ is the electrostriction coefficient (see the Appendix for exact definitions of $\xi$ and $c$).

For non-oriented films, $\alpha = 0.5$. Thus, by substituting this value into Eq. 5, it follows that

$$S_\sim = \frac{\xi}{c}\left(E_0E_{10}\cos \omega t + \frac{1}{2}E_{10}^2 \cos 2\omega t\right), \tag{6}$$

i.e., the first harmonics of the deformation (and the transformation function $k_{1\to2}(U_0)$ according to its definition in Eq. 1) is proportional to the applied external field $E_0$. It is evident that non-oriented films do not emit the first-harmonic acoustic waves when $E_0 = 0$. The phase difference between the excitation signal $E_{1\sim}$ and the deformation response $S_\sim$ changes by 180° when the direction of $E_0$ is changed, which is reflected in Eq. 6 as the change in the sign of the amplitude of the first harmonics. The second harmonics of the deformation (see Eq. 6) is independent of the external DC voltage $U_0$ (as well as $E_0$) as is seen in Fig. 4. From this definition of the transformation function, Eq. 6 also implies the quadratic dependence of the amplitude of the second harmonics of deformation on the amplitude of the excitation signal $U_{10}$, which is indeed observed (see Fig. 5).

From the comparison of experimental observations with the model presented in the Appendix, the dependence of deformation on the electric field in PMs can be entirely described as a parabolic function (see Eq. 5). Considering the fact that the deformation is positive (the thickness of the film decreases) regardless of the direction of the external electric field, according to Eq. A.2, the electrostriction coefficient has to be positive ($d\varepsilon/d\rho > 0$).

For the films with partly or highly oriented PMs, $\alpha > 0.5$. Thus, the first term in Eq. 5 that gives the first harmonics is nonzero even at $E_0 = 0$ and both the DC voltage field $E_0$ and the internal membrane field $E_m$ determine the conditions of the first harmonics generation, shown in Fig. 3. For partly oriented films $0.5 < \alpha < 1$, from Eq. 5 it follows that the amplitude of the first harmonics is zero when $E_0 = -(2\alpha - 1)E_m$. Such a shift of the minimum of the first harmonics amplitude is indeed seen in Fig. 3, where the results are shown for the films with different degrees of PM orientation.

For highly oriented films, we can roughly assume that $\alpha = 1$. Then the minimum of the first harmonics amplitude corresponds to the condition $E_0 = -E_m$, which means that the external DC voltage has to compensate for the internal cross-membrane electric field. Due to very high values of the latter, this minimum was not reached experimentally. However, by extrapolating the experimental data to the intersection point with the $E_0$ axis, the cross-membrane field can be determined, and, from experimental data for highly oriented films, it was found to be equal to $E_m \approx -10^8$ V/cm. The minus sign means that the external (endoplasmic) surface of the PM has to be charged negatively. The accuracy of the value of the cross-membrane field determined in this way depends entirely on how well PMs are oriented within the film. Furthermore, in the absence of the external field $E_0$, for the first harmonics of deformation, Eq. 5 yields

$$S_\sim = \frac{\xi}{c} \cdot E_mE_{1\sim}. \tag{7}$$

This result demonstrates the relationship between the piezoelectricity and the electrostriction effect for the PM films, the surfaces of which are charged. The piezoelectric coefficient is then proportional to the value of the cross-membrane field.

## Direct piezoelectric effect

The cross-membrane field $E_m$ arises from the polarization $P_m$, which is caused by the charges bound on the surfaces of

the membrane. Provided the density of bound charges is constant, polarization cannot be changed by the deformation. Polarization is related to the cross-membrane electric field and the membrane susceptibility $\varepsilon$ by the equation,

$$\varepsilon_0 \varepsilon E_m = P_m. \tag{8}$$

Calculating the derivative of Eq. 8 assuming that $P_m$ is constant, (this is justified if the change in the mass density is mainly due to the changes in the thickness of the membrane), we find,

$$E_m \frac{d\varepsilon}{d\rho} = -\varepsilon \frac{dE_m}{d\rho}. \tag{9}$$

Under our experimental conditions, the change in the cross-membrane field is caused by the (weak) AC field $E_{\sim}$; therefore, let us assume $dE_m \cong E_{1\sim}$. Considering also the definition of the density as $\rho = m/V$, where $m$ is a mass of the membrane enclosed in the volume $V$, and supposing that the mass is fixed, we obtain

$$d\rho = -(m/V^2)dV \equiv \rho S. \tag{10}$$

Here $S = -dV/V$, because, as mentioned above, for thin membranes the variation of the volume is mainly caused by the changes in the thickness. Substituting Eq. 10 into the right-hand side of Eq. 9, the variation of the cross-membrane field is expressed as

$$E_{1\sim} = -\frac{1}{\varepsilon} \rho \frac{d\varepsilon}{d\rho} E_m S. \tag{11}$$

In the case when the external DC field is applied to the membrane, it must be added to the value $E_m$ in Eq. 11. The above equations are valid for the stand-alone membrane, whereas for dry films, the orientation parameter $\alpha$ must also be introduced in the same way as in Eq. 4. Incorporation of the orientation parameter and the externally applied DC field in Eq. 11 can be generalized as

$$E_{1\sim} = -\frac{1}{\varepsilon} \rho \frac{d\varepsilon}{d\rho} [E_m(2\alpha - 1) + E_0] S_{\sim}. \tag{12}$$

Eq. 12 explains striking similarities between Figs. 2 and 6. For all types of the PM films, the obtained values of the external field $E_0$, where the electric response to the deformation vanishes in Fig. 6, are the same as the values where the mechanical response to the electric field crosses zero in Fig. 2. This is because the terms in square brackets in Eq. 5 and Eq. 12 are the same. The other feature explained by the formalism presented above is the phase difference between excitation and response signals in both cases. The minus sign in Eq. 12 shows that, in Fig. 6 as compared to Fig. 2, the response curve should be inverted, which is clearly reproduced in our experiments.

Referring to the above considerations, piezoelectric properties of PM films shown in Figs. 1–6 can be understood as a result of electrostriction and electric asymmetry of purple membranes.

## General

On the basis of the results described above, the following model of the PM function related to this mechanical-to-electrical coupling property can be formulated. As was already mentioned in Materials and Methods (see subsection Sample preparation) the oriented films are visually distinguishable from the non-oriented films. The oriented ones are blue and their absorption spectra are shifted to red by 15–20 nm in comparison with the absorption of BR under normal conditions (at 570 nm). This shift can be attributed to the environment pH = 3 ÷ 5 (Oesterhelt and Stoeckenius, 1971), whereas the photoactivity of BR under these conditions remains unchanged (Moltke and Heyn, 1995). It was shown (Jonas et al., 1990; Mostafa et al., 1995; Taneva and Petkanchin, 1999) that the dipole moment of the PM strongly increases at these values of pH. This results from the changed balance of the surface charges, i.e., the external surface becoming more negative than the internal side. This is in line with our model, which is based on the assumption of the presence of the intrinsic electric field ($E_m$) in the PM caused by the electric asymmetry (differences in charges bound on the surfaces) of the membrane. This asymmetry is schematically shown in Fig. 7 by suggesting that the external side of the membrane has bound negative and the internal side-positive charges.

Because of the electrostrictive properties of the membranes, the intrinsic cross-membrane field $E_m$ causes the

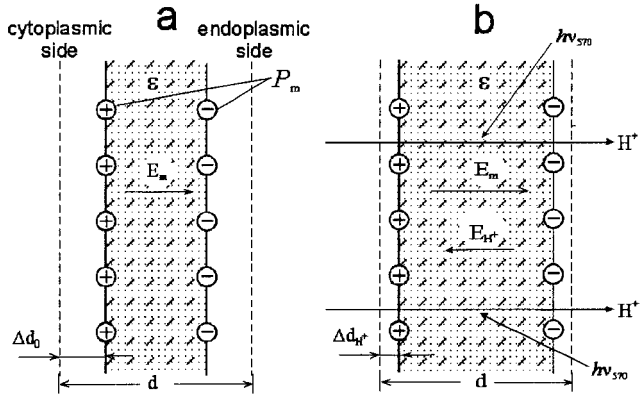


FIGURE 7 Electromechanical model of the membrane in the presence (*A*) and in the absence (*B*) of external illumination. The membrane has intrinsic electric asymmetry $P_m$. Due to the electrostrictive properties of the membrane, this asymmetry causes the thickness of the membrane to decrease from the value $d$ (which would describe the hypothetical electrically symmetric membrane) to the value $d - \Delta d_0$. When light initiates the proton transfer to the endoplasmic side of the membrane (see panel *B*), the resulting cross-membrane field partly compensates the intrinsic membrane field and causes the thickness to relax to $d - \Delta d_{H^+}$. Note that this relaxation can also be caused by the externally applied electric field.

contraction of the membrane even in the absence of the external DC voltage $U_0$ (see Fig. 7 *A*), which explains the results shown in Fig. 3 in the case of highly oriented membranes. When the externally applied field has the same direction as the internal field $E_m$ (negative voltage is connected to the endoplasmic side), the films are squeezed even more, and vice versa, i.e., when the external field is opposite to the intrinsic membrane field, the membrane relaxes and its thickness increases.

Optical excitation of the PM generates the proton pumping across the membrane toward the external (endoplasmic) side and the resultant cross-membrane field decreases. According to the electrical-to-mechanical coupling model suggested above, the thickness of the membrane should increase then (see Fig. 7 *B*). Qualitatively, this is in line with recent observations of the changes in the thickness of the films (Rousso et al., 1997a,b). The excitation light at 570 nm causes the proton transfer across the membrane and hence the thickness of the membrane increases. By using an additional excitation at 412 nm, the proton transfer cycle is disturbed, and the impact of the proton transfer on the electric cross-membrane field decreases (Rousso et al., 1997a). According to our model based on the electrostriction effect, the thickness of the membrane then has to decrease.

The experiments presented in this study clearly show that electrical and mechanical phenomena in PM films (hence, in stand-alone membranes) are coupled. Our hypothesis is that this coupling could play a significant role in the functioning of BR creating the main driving force of charge separation. The illustration of how this process can take place is shown in Fig. 8. Initially the proton resides on the Schiff base (*SB*) separated from the acceptor (*Ac*) by an energy barrier $W_a$ (Fig. 8 *A*). Upon excitation, the dipole moment is induced in the retinal molecule (it is accompanied by the changes in the geometrical structure—isomerization), which creates a polarization field represented by the potential difference $U_p$. Due to the mechanical-to-electrical coupling, the change in the cross-membrane field results in deformation (reorganization) of the protein. Upon the deformation, the distance between the proton position at the Schiff base and the proton accepting group decreases, and the height of the energy barrier changes down to $W_{ad}$ within some time ($\tau_1$). This time is determined by the inertia and friction (viscosity) that tamper with the movement of $\alpha$-segments of the protein. Moreover, according to Eq. 11, the field $U_p$ distorts the barrier, making it asymmetric in favor of the proton transfer to Ac (Fig. 8 *B*). At this point, the intermediate of BR is electrogenic because the negative charge is induced on the endoplasmic side of the membrane (Fig. 9). Due to the asymmetry and the decrease in the energy barrier, the SB deprotonation takes place within some characteristic time $\tau_2$. The resulting electric field created by the transferred proton $U_{H^+}$ partly or fully compensates the polarization field $U_p$ and restores the symmetry of the energy barrier (Fig. 8 *C*). Hence, the intermediate C of BR has to be electrically neutral. After some time ($\tau_3$), the polarization field $U_p$ relaxes and the initial size of the barrier is restored. However, now the barrier is asymmetric again due to the cross-membrane field created by the transferred proton. The height of the barrier increases back to its initial value $W_a$, which holds the proton from returning to its initial position at the Schiff base (Fig. 8 *D*). To summarize, the proton driving force is a result of this mechanical-to-electrical coupling, which results in positive charge generation on the external side of the membrane when the whole sequence of events finishes (Fig. 9).

The sequence of the intermediates reflecting the light energy conversion according to our model is as follows. The absorbed photon at the very initial stages creates the mechanical tension in the protein, the energy of which is converted after some time into the energy of deformation and the created electric field (B intermediate). The proton translocation during the next stage (C intermediate) compensates the electric field, which results in the decrease of the proton energy. Thus, it is evident that the proton itself does not gain energy and remains energetically relaxed in A, B, and C intermediates. However, at stage D, when only the potential energy of the proton $U_{H^+}$ is remaining and the polarization energy $U_p$ relaxes, the whole deformation energy concentrated at stage B is delivered to the proton. This allows us to attribute the proton driving force to the deformation of the protein as the result of the electrical-to-mechanical coupling.

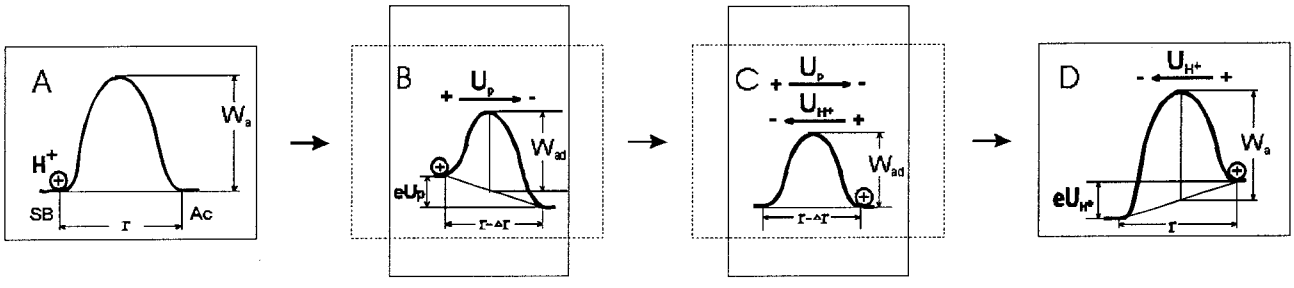


FIGURE 8 Illustration of the mechanical-to-electrical coupling acting as a driving force in charge separation in BR. For details see text.

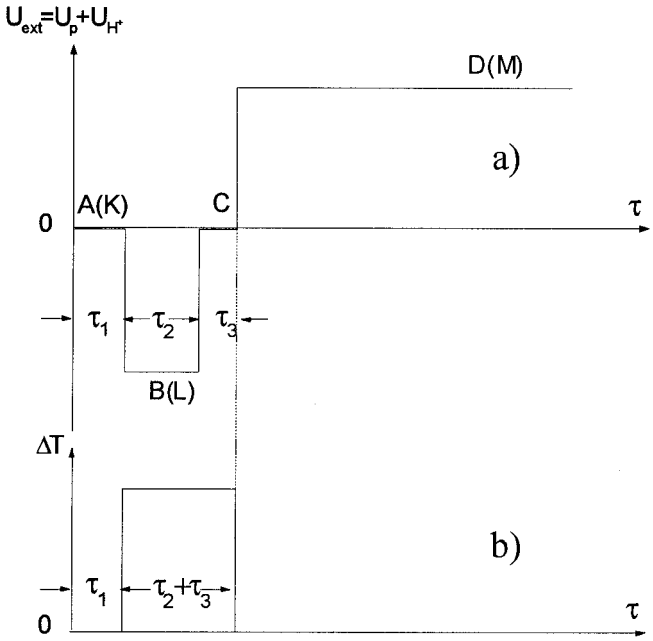


FIGURE 9 Kinetics of the electric potential ($U_{ext} = U_p + U_{H^+}$) of (*A*) a single BR molecule and (*B*) the changes in transparency ($\Delta T$) of a single BR molecule for the proton transfer. The time constants for different intermediates of BR are also shown. The correspondence of the states A, B, C, and D to the spectroscopically determined intermediates K, L, and M are presented in brackets.

The electrogenicity of our postulated states A, B, C, and D for the separate BR molecule and possible correspondence of these states to the intermediates K, L, and M, known from the spectroscopic studies, are represented in Fig. 9. For a separate PM, the effective potential change ($U_{ext}$) on the external surface of the membrane is shown in Fig. 9 *A*, whereas changes in the BR transparency for the proton transfer in the different intermediate stages is shown in Fig. 9 *B*. The latter dependence of the transparency for the proton transmittance directly resembles the changes of the energy barrier as shown in Fig. 8. To describe the transition between these states in the ensemble of such molecules, the following kinetic equations have to be considered:

$$\frac{d[A]}{dt} = -\frac{[A]}{\tau_1}, \quad \frac{d[B]}{dt} = \frac{[A]}{\tau_1} - \frac{[B]}{\tau_2},$$
$$\frac{d[C]}{dt} = \frac{[B]}{\tau_2} - \frac{[C]}{\tau_3}, \quad \frac{d[D]}{dt} = \frac{[C]}{\tau_3}, \tag{13}$$

where $[X]$ is the concentration of the BR molecules in *X*-state. Moreover, the condition, $[A] + [B] + [C] + [D] = N^*_{BR}$, has to be fulfilled, $N^*_{BR}$ being the concentration of the optically excited BR molecules.

The origin of the A and C intermediates is related to rise and vanishing of the molecular deformation according to our model. Therefore, we can suggest that $\tau_1 \approx \tau_3$ and thus both these values equal to $\tau_K \approx 2$ $\mu$s, while $\tau_2 = \tau_L$ and $\tau_L \approx 50$ $\mu$s according to the lifetimes of the photochemical intermediates K and L of BR (see, for instance Trissl, 1990; Mathies et al., 1991). Because B and D intermediates are electrogenic when the changes in the potential ($U_{BR*} = U_p + U_{H^+}$) take place, the electric response to the optical excitation can be determined as the difference of the concentrations of the BR in states D and B. Similarly, the kinetics of the changes in conductivity in the ensemble of PMs $\Delta\sigma$ caused by the transmittance effect (transparency) of the single BR (see Fig. 9 *B*) can be determined as a sum of BR molecules being populated in B and C states. Thus,

$$U_{BR*} \propto [D] - [B], \quad \Delta\sigma \propto [B] + [C]. \tag{14}$$

By solving Eq. 13 for the case of short excitation pulses, i.e., when the pulse duration is much shorter than $\tau_1$, the result can be easily obtained, giving the kinetics shown in Fig. 10, which qualitatively resembles the experimental observations (see, for instance Trissl, 1990, and McIntosh and Boucher, 1991). Thus, the model presented above gives a general illustration of how the electrical-to-mechanical coupling can drive the charge transfer in BR.

## CONCLUSIONS

In this study, we have demonstrated the electrical-to-mechanical coupling in PM films. This coupling manifests itself experimentally as the direct and inverse piezoelectric effect of these films. It has been shown that both these effects are caused by the electric asymmetry of PMs and electrostriction. The experiments performed on the oriented samples allow determination of the value of the cross-membrane electric field.

We hypothesize that the electrical-to-mechanical coupling is the main driving force for the proton transfer against

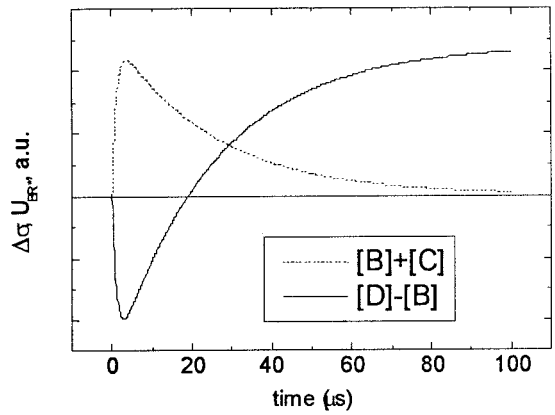


FIGURE 10 Kinetics of the electric potential $U_{BR*}$ (*solid line*) and the time dependence of the changes of conductivity $\Delta\sigma$ (*dashed line*) in the ensemble of BR molecules according to the model, shown in Fig. 8. The following time constants are used for calculations: $\tau_1 = \tau_3 = 2$ $\mu$s, $\tau_2 = 50$ $\mu$s.

Coulomb forces in the membrane, in other words, this coupling is the main source of electrogenicity of PM. This working hypothesis, however, has to be further tested by other acousto-electrical and spectroscopic experiments. Experiments directed to detect the electrical-to-mechanical coupling in other photoactive pigment-protein complexes could answer whether this phenomenon is common to the pigment-protein complexes involved in the charge transfer across the biological membranes.

## APPENDIX: THE MAIN EXPRESSIONS FOR ELECTROSTRICTION

Let us briefly describe the main standpoint of electrostriction. The force ($f$) acting on the unit area of the dielectric medium in the electric field is determined by (Landau and Lifshitz, 1960)

$$f = -\frac{1}{2}\varepsilon_0 E^2 \nabla\varepsilon + \frac{\varepsilon_0}{2}\nabla\left(\rho\frac{d\varepsilon}{d\rho}E^2\right), \quad \text{(A1)}$$

where $\varepsilon_0$ is the dielectric constant, $\rho$ is the material density of the film, $\varepsilon$ is the dielectric susceptibility and $E$ is the strength of the electric field inside the dielectric media. The first term results from the spatial inhomogeneity of the dielectric susceptibility. For the dielectric plate present in the electric field, this force would appear at the separating boundary between the plate and its environment. The second term in Eq. A1 is caused by the dependence of the dielectric susceptibility on the density of the matter $\rho$. The integral of the second term over the whole volume of the dielectric body is zero, so that this force cannot change the position of the body in space. However, this force causes the mechanical tension of the dielectric medium in the presence of the external electric field; this phenomenon is known as electrostriction. The density of electrostriction forces in the homogeneous medium is evenly distributed within the volume, and, in this sense, this phenomenon is similar to the inverse piezoelectric effect. For one-dimensional plate, the mechanical tension ($T$) per surface unit can be calculated from Eq. A1 as

$$T = \frac{\varepsilon_0}{2}\rho\frac{d\varepsilon}{d\rho}E^2. \quad \text{(A2)}$$

This force of the mechanical stress is compensated by the hydrodynamical pressure in fluids and gases, and by elasticity in solid states.

According to the Hooke's law, $T = cS$, where $c$ is the elasticity and $S$ is the deformation. Then, by using Eq. A2, it follows that

$$S = \frac{\xi}{2c}E^2, \quad \text{(A3)}$$

where

$$\xi = \varepsilon_0\rho\frac{d\varepsilon}{d\rho} \quad \text{(A4)}$$

is the so-called electrostriction coefficient. The positive sign of deformation ($S > 0$) means the contraction of the dielectric plate, whereas, in the opposite case ($S < 0$), it is expanded. Because this sign is independent of the direction of the external electric field (thus, for the media characterized by $d\varepsilon/d\rho > 0$), the volume decreases in the presence of the external electric field. Materials characterized by the negative electrostriction coefficient ($d\varepsilon/d\rho < 0$) expand in the electric field.

Dr. Z. Dancshazy and Dr. S. Varo are gratefully acknowledged for the assistance with the preparation of PM films.

This research was partially supported by the Lithuanian Foundation of Science and Studies.

## REFERENCES

Balashov, S. P., E. S. Imasheva, T. G. Ebrey, N. Chen, D. R. Menick, and R. K. Crouch. 1997. Glutamate-194 to cysteine mutation inhibits fast light-induced proton release in bacteriorhodopsin. *Biochemistry.* 36: 8671–8676.

Belrhali, E., P. Nollert, D. Royant, C. Menzel, J. R. Rosenbusch, E. M. Landau, and E. Pebay-Peyroula. 1999. Protein, lipid and water organization in bacteriorhodopsin: a molecular view of the purple membrane at 1.9 angstroms resolution. *Structure.* 7:909–917.

Brown, L. S., J. Sasaki, H. Kandori, A. Maeda, R. Neederman, and J. K. Lanyi. 1995. Glutamatic acid 204 is the terminal proton release group at the extracellular surface of bacteriorhodopsin. *J. Biol. Chem.* 270: 27122–27126.

Cao, Y., L. S. Brown, J. Sasaki, A. Maeda, R. Neederman, and J. K. Lanyi. 1995. Relationship of proton release at the extracellular surface to deprotonation of the Schiff base in the bacteriorhodopsin photocycle. *Biophys. J.* 68:1518–1530.

De Groot, H. J. M., G. S. Harbison, J. Herzfeld, and R. G. Griffin. 1989. Nuclear magnetic resonance study of the Schiff base in bacteriorhodopsin: counterion effects on the 15N shift anisotropy. *Biochemistry.* 28:3346–3353.

De Groot, H. J. M., S. O. Smith, J. Courtin, E. van der Berg, C. Winkel, J. Lugtenburg, R. G. Griffin, and J. Herzfeld. 1990. Solid-state 13C and 15N NMR study of the low pH forms of bacteriorhodopsin. *Biochemistry.* 29:6873–6883.

Essen, L. O., R. Siegert, W. D. Lehmann, and D. Oesterhelt. 1998. Lipid patches in membrane protein oligomers: crystal structure of the bacteriorhodopsin–lipid complex. *Proc. Natl. Acad. Sci. USA.* 95: 11673–11678.

Ganea, C., C. Gergely, K. Ludmann, and G. Varo. 1997. The role of water in the extracellular half channel of bacteriorhodopsin. *Biophys. J.* 73: 2718–2725.

Heberle, J., and N. A. Dencher. 1992. Surface-bound optical probes monitor proton translocation and surface potential changes during the bacteriorhodopsin photocycle. *Proc. Natl. Acad. Sci. USA.* 89:5996–6000.

Jonas, R., Y. Kontalos, and T. G. Ebrey. 1990. Purple membrane: surface chare density and the multiple effect of pH cations. *Photochem. Photobiol.* 52:1163–1177.

Kietis, P. 1984. Piezoelectric mechanism of charge in the purple membranes of *Halobacterium halobium. Biol. Membranes* (in Russian). 1:1304–1315.

Kietis, P. B., and R. Rozga. 1987. Strained conformation and active transport of ions in bacteriorhodopsin. *Biol. Membranes* (in Russian). 4:613–623.

Kietis, P., D. Linge, S. Pakalnis, and L. Valkunas. 1998a. Piezoelectric model of energy transformation in bacteriorhodopsin. *Lith. J. Phys.* 38:313–319.

Kietis, P., R. Valiokas, D. Linge, and L. Valkunas. 1998b. Nonlinear piezoelectric effect in the purple membrane of bacteriorhodopsin. *Lith. J. Phys.* 38:93–97.

Kietis, P., M. Vengris, and L. Valkunas. 1999. Electrical-mechanical coupling and active charge transport in dry films of purple membranes. *Environ. Chem. Phys.* 21:109–115.

Kimura, Y., D. G. Vassylyev, A. Miyazawa, A. Kidera, M. Matsushima, K. Mitsuoka, K. Murata, T. Hirai, and Y. Fujiyoshi. 1997. Surface of bacteriorhodopsin revealed by high-resolution electron crystallography. *Nature.* 389:206–211.

Landau, L. D., and E. M. Lifshitz. 1960. Electrodynamics of Continuous Media. Pergamon Press, Oxford, U.K. 36–91.

Lanyi, J. K. 1993. Proton translocation mechanism and energetics in the light-driven pump bacteriorhodopsin. *Biochim. Biophys. Acta.* 1183: 241–261.

Lu, M., S. P. Balashov, T. G. Ebrey, N. Chen, Y. Chen, D. R. Menick, and R. K. Crouch. 2000. Evidence for the rate of the final step in the bacteriorhodopsin photocycle being controlled by the proton release group: R134H mutant. *Biochemistry.* 39:2325–2331.

Ludmann, K., C. Gergely, A. Der, and G. Varo. 1998a. Electric signals during the bacteriorhodopsin photocycle, determined over a wide pH range. *Biophys. J.* 75:3120–3126.

Ludmann, K., C. Gergely, and G. Varo. 1998b. Kinetic and thermodynamic study of the bacteriorhodopsin photocycle over a wide pH range. *Biophys. J.* 75:3110–3119.

Luecke, H., B. Schobert, H.-T. Richter, J.-P. Cartailler, and J. K. Lanyi. 1999. Structure of bacteriorhodopsin at 1.55 A resolution. *J. Mol. Biol.* 291:899–911.

Mathies, R. A., S. W. Lin, J. B. Ames, and W. T. Pollard. 1991. From femtoseconds to biology: mechanism of bacteriorhodopsin's light-driven proton pump. *Annu. Rev. Biophys. Biophys. Chem.* 20:491–518.

McIntosh, A. R., and F. Boucher. 1991. Photochemically induced charge separation occurring in bacteriorhodopsin. Detection by time-resolved dielectric loss. *Biophys. J.* 60:1–7.

Moltke, S., and M. P. Heyn. 1995. Photovoltage kinetics of the acid-blue and acid-purple forms of bacteriorhodopsin: evidence for no net charge transfer. *Biophys. J.* 69:2066–2073.

Mostafa, H. I. A., G. Varo, R. Toth-Boconadi, A. Der, and L. Keszthelyi. 1996. Electrooptical measurements on purple membrane containing bacteriorhodopsin mutants. *Biophys. J.* 70:468–472.

Oesterhelt, D., and W. Stoeckenius. 1971. Rhodopsin-like protein from the purple membrane of *Halobacterium halobium. Nature New Biol.* 233: 149–152.

Oesterhelt, D., J. Tittor, and E. Bamberg. 1992. A unifying concept for ion translocation by retinal proteins. *J. Bioenerg. Biomembr.* 24:181–191.

Pasechnik, V. I. 1982. Electrostrictive measurements of viscous-elastic properties of lipid bilayer membranes. *In* Itogi Nauki i Tekchniki (in Russian). Vol. 2. P. G. Kostjuk, editor. VINITI, Moscow. 267–307.

Popp, A., M. Wolperdinger, N. Hampp, C. Bräuchle, and D. Oesterhelt. 1993. Photochemical conversion of the O-intermediate to 9-*cis*-retinal-containing products in bacteriorhodopsin films. *Biophys. J.* 65: 1449–1459.

Rothschild, K. J. 1992. FTIR difference spectroscopy of bacteriorhodopsin—toward a molecular model. *J. Bioenerg. Biomembr.* 24:147–167.

Rousso, I., E. Khatchatryan, I. Brodsky, R. Nachustai, M. Ottolenghi, M. Sheves, and A. Lewis. 1997a. Atomic force sensing of light-induced protein dynamics with microsecond time resolution in bacteriorhodopsin and photosynthetic reaction centers. *J. Struct. Biol.* 119:158–164.

Rousso, I., E. Khatchatryan, Y. Gat, I. Brodsky, M. Ottolenghi, M. Sheves, and A. Lewis. 1997b. Microsecond atomic force sensing of protein conformational dynamics: implication for the primary light-induced events in bacteriorhodopsin. *Proc. Natl. Acad. Sci. USA.* 94:7937–7941.

Trissl, H.-W. 1990. Photoelectric measurements of purple membranes. *Photochem. Photobiol.* 51:793–818.

Varo, G. 1981. Dried oriented purple membrane samples. *Acta Biol. Acad. Sci. Hung.* 32:301–310.

Varo, G., and J. K. Lanyi. 1991. Kinetic and spectroscopic evidence for an irreversible step between deprotonation and reprotonation of the Schiff base in the bacteriorhodopsin photocycle. *Biochemistry.* 30:5008–5015.

Wang, J.-P., S.-K. Yoo, L. Song, and M. El-Sayed. 1997. Molecular mechanism of the differential photoelectric response of bacteriorhodopsin. *J. Phys. Chem. B.* 101:3420–3423.

Zimanyi, L., G. Varo, M. Chang, B. Ni, R. Neederman, and J. K. Lanyi. 1992. Pathways of proton release in the bacteriorhodopsin photocycle. *Biochemistry.* 31:8535–8543.